Analysis of Piecewise Linear Aeroelastic Systems Using Numerical Continuation

I. Roberts D. P. Jones N. A. J. Lieven M. di Bernado† A. R. Champneys†
Departments of Aerospace Engineering & †Engineering Mathematics,
Bristol University, Bristol, BS8 1TR, England

October 24, 2001

Abstract

This paper demonstrates the application of a numerical continuation method to dynamic piecewise aeroelastic systems. The aeroelastic system is initially converted into a state space form, and then into a set of equations which solve the system as the motion moves between different linear zones in a freeplay motion. Once an initial condition is found that satisfies these sets of equations a continuation method is used to find all other possible solutions of the same period for a variation in any parameter. This process can then be repeated for different order systems allowing the limit cycle behaviour of the whole system to be built up. The solutions found using this method have been shown to be the same as those found using a more traditional Runge-Kutta type approach with a considerable time saving and added flexibility through multiple parameter variation.

1 Introduction

Recent activities in fixed wing aeroelasticity have concentrated on the identification of limit cycle oscillations (LCOs) in nonlinear systems [1, 2, 3, 4, 5, 6, 7]. Much of this work has concentrated on improved aerodynamics especially in the transonic regime. Various approaches have been taken to reduce the often complex computational aerodynamics [8, 9]. However, the

focus of the work in this paper is to study the structurally nonlinear aspects of the aeroelastic problem.

The main structural nonlinearities that occur are cubic stiffening and freeplay (or backlash) which are illustrated in figures 1 and 2 respectively [1, 2]. Cubic stiffening occurs in all degrees of freedom and is usually due to large amplitude oscillations and therefore is only significant during high acceleration manoeuvres or extreme dynamic responses. Freeplay nonlinearities, which shall be studied in this paper, occur in the actuated degrees of freedom, i.e. in the control surfaces or components with loose joints. The amount of freeplay within the system is usually small in the region of 0.2 degrees [2]. However, this small amount of freeplay is highly problematic as any amount can cause limit cycle oscillations of the whole structure. Although the structural motion is usually relatively small, the effects of fatigue on the structure are of concern. The next generation of combat aircraft is also intended to push the flight envelope further, resulting in performance requirements closer to the flutter boundary. It is in this region of the flight envelope where the LCO amplitudes due to freeplay become of significant concern.

The conventional method for studying limit cycles is to perform numerous simulations using Runge-Kutta type time integration. The accuracy of these runs, for freeplay, depends on the precise capture of the switching times between the zones. Capture of these switching times often requires a computationally expensive iteration, the expense can be significantly reduced however, using a single back step via Hénon's method [3]. Other methods of solving for structural nonlinearities are currently being researched by it Sedaghat et al. [4]. The method uses the simplified integro-differential method of Fung [10] and finds solutions using the Normal Form Theory. Much work in this area has also been performed by Alighanbari and Price [5] who utilised the AUTO continuation software to solve for a rational curve approximation to the freeplay nonlinearity. With the exception of the Runge-Kutta methodology all the systems discussed are restricted to continuous nonlinearities and, to analyse piecewise linear systems, require a curve approximation. The inability to capture the switching points accurately results in round off errors which may lead to numerical instability of the whole system [6] which leads, in turn, to incorrect solutions to the problem.

This paper presents a method of accurately identifying and classifying limit cycles in a two-dimensional, three degree-of-freedom aeroelastic system by partitioning the equations of motion into their three distinct linear regions. The further manipulation of the system of equations into state space form results in a set of equations which is then used in a continuation method to

track a period-*n* oscillation throughout the flight envelope. The study also stresses the usefulness of the adopted approach as a design tool where any parameter may be varied and its consequential effects on the existence of the LCOs analysed. Boundary capturing similar to that described here has also recently been presented by Wong et al. [11] using a Point Transformation (PT) method and an alternative form of aerodynamic model.

The aerodynamic model used in this particular study assumes, low speed, two-dimensional flow [12] to demonstrate the effectiveness of numerical continuation in aeroelastic simulation. The technique can be applied to any aerodynamic model that can be represented in state space form. Furthermore, the method is equally valid for any form of piecewise linear equations in state space form including systems with offsets, impacts or relayed control switches.

2 Theory

2.1 General Problem Description

The methodology developed uses the simple fact that a piecewise linear system is constructed from of a set of linear systems. Hence state space can be divided into discretezones where different linear systems apply. The zones are separated by jump conditions that piece together the different dynamics. If the time and state variables are known as the motion enters each zone it is possible to analytically calculate the resultant motion up to the point that the state reaches the boundary with another zone.

Let us now describe how the state space model derived by Edwards et al. [12] can be used to define a new nonlinear system which is linear in each zone. The state variables used are heave, pitch, control-surface rotation ($y = [\xi, \alpha, \beta]^T$), their derivatives with respect to time and two augmented aerodynamic states that shall be called, s_1 and s_2. The augmented aerodynamic states are required for Jones' representation of the generalised Theodorsen function through the approximation of Wagner's indicial loading function. For this particular case, a *backlash* (or freeplay) nonlinearity as shown in figure 2 in flap rotation for the system shown in figure 3 is assumed.

The general equations of motion for such a system are,

$$[M]\ddot{\boldsymbol{y}} + [B]\dot{\boldsymbol{y}} + [K]\boldsymbol{y} = \boldsymbol{F} \tag{1}$$

Where $[M]$, $[B]$, and $[K]$ are the mass, damping and stiffness matrices respectively. $\boldsymbol{F}$ is a vector made up of lift, moment about the quarter chord and moment about the control surface hinge. Using the aerodynamic theory stated by Edwards et al. [12], this can be converted into a system of equations of the form,

$$\begin{pmatrix} \dot{y} \\ \ddot{y} \\ \dot{s}_1 \\ \dot{s}_2 \end{pmatrix}_{8\times1} = \begin{bmatrix} 0 & I & 0 \\ -M_{tot}^{-1}K_{tot} & -M_{tot}^{-1}B_{tot} & M_{tot}^{-1}D \\ E_1 & E_2 & F_p \end{bmatrix}_{8\times8} \begin{pmatrix} y \\ \dot{y} \\ s_1 \\ s_2 \end{pmatrix}_{8\times1} \tag{2}$$

The matrices $[E_1]$, $[E_2]$, $[F_p]$ and $[D]$ are matrices solely linked to aerodynamic variables whereas $[M_{tot}]$, $[K_{tot}]$ and $[B_{tot}]$ are a combination of aerodynamic and structural matrices.

If the system then includes a backlash nonlinearity in the flap rotation, the equations become of the form,

$$\dot{\boldsymbol{x}} = [A]\cdot\boldsymbol{x} + \boldsymbol{b}\begin{cases} \boldsymbol{b} = \boldsymbol{b}_1 & \text{and} \quad [A] = [A_1] \quad \text{for} \quad \beta \le -\frac{\delta}{2}, \\ \boldsymbol{b} = \boldsymbol{0} & \text{and} \quad [A] = [A_2] \quad \text{for} \quad -\frac{\delta}{2} < \beta < \frac{\delta}{2}, \\ \boldsymbol{b} = -\boldsymbol{b}_1 & \text{and} \quad [A] = [A_1] \quad \text{for} \quad \beta \ge \frac{\delta}{2}. \end{cases} \tag{3}$$

Where the vector $\boldsymbol{b}$ accounts for the outer zones not going through the origin of the graph (zones (1) and (3) in figure 2). $[A]$ is the matrix in equation (2) with the differences between the zones due to the structural stiffness component in the β degree-of-freedom being zero in the freeplay region (represented by $[A_2]$). This form of the equation makes it possible to calculate the time and state of the system as it switches between the zones.

2.2 Boundary Identification

Given the general linear state space equation,

$$\dot{\boldsymbol{x}} = [A]\cdot\boldsymbol{x} + \boldsymbol{b} \tag{4}$$

where,

$$\boldsymbol{x} = [\xi, \alpha, \beta, \dot{\xi}, \dot{\alpha}, \dot{\beta}, s_1, s_2]^T \tag{5}$$

the generalised solution is given as,

$$\boldsymbol{x}(t) = e^{[A]t}(\boldsymbol{x}(0) + [A]^{-1}\boldsymbol{b}) - [A]^{-1}\boldsymbol{b} \tag{6}$$

where $\boldsymbol{x}(0)$ is the set of initial conditions as the motion enters the linear area.

To solve the system, the time at which $\beta = \pm\frac{\delta}{2}$ must be found as these represent the boundaries between zones. Solving equation (6) for *t,* the vector transpose $\boldsymbol{c}$ is of the form,

$$\boldsymbol{c} = [0, 0, 1, 0, 0, 0, 0, 0] \tag{7}$$

and isolates the β degree of freedom. This results in,

$$\pm\frac{\delta}{2} = \boldsymbol{c}e^{[A]t}(\boldsymbol{x}(0) \pm [A]^{-1}\boldsymbol{b}) \mp \boldsymbol{c}[A]^{-1}\boldsymbol{b} \tag{8}$$

The evaluation of $e^{[A]t}$, the exponential of a matrix [13], is given by,

$$e^{[A]} = [V][e^{\boldsymbol{G}}][V]^{-1} \tag{9}$$

where $[V]$, $\boldsymbol{G}$ and $[e^{\boldsymbol{G}}]$ respectively represent the eigenvectors of $[A]$, the vector of eigenvalues of $[A]$ and the diagonal matrix where entries are exponentials of the eigenvalues.

$$[G] = \begin{bmatrix} \lambda_1 & 0 & \dots & 0 \\ 0 & \lambda_2 & \dots & 0 \\ \vdots & \vdots & \ddots & 0 \\ 0 & 0 & \dots & \lambda_8 \end{bmatrix} \tag{10}$$

$$e^{[G]} = \begin{bmatrix} e^{\lambda_1} & 0 & \dots & 0 \\ 0 & e^{\lambda_2} & \dots & 0 \\ \vdots & \vdots & \ddots & 0 \\ 0 & 0 & \dots & e^{\lambda_8} \end{bmatrix} \tag{11}$$

Rearranging equation (8), we are left with a solution of the form,

$$0 = \sum_{i=1}^{n} a_i e^{\lambda_i t} \pm \frac{\delta}{2} \tag{12}$$

where t is the only unknown. Here λ_i are the eigenvalues of A and a_i are formed from a combination of $[A]$, $[V]$, $[V]^{-1}$ and $\boldsymbol{b}$. Note that equation (12) is nonlinear in t and, in general, no unique solution exists. To solve such a problem one must typically resort to some form of numerical root-finding routine. The problem was simulated in *Matlab*, therefore it was obvious

that the internal solvers *fsolve, fzero* and *fmincon* [14, 15] should be used. *fsolve* and *fzero* are subroutines that find a zero of a function using a least squares algorithm and a bisection method respectively [14, 15]. *fmincon* finds the minimum of a function within a specified range using the subspace trust region method based on the interior-reflective Newton method [15]. With these programs it becomes possible to solve an equation, such as (8), for the unknown variable *t*. However, The methodology outlined above is quite time consuming due to the ineffectiveness of the methods used in the functions.

2.3 Numerical Continuation Method

A continuation method such as that used in the software AUTO [16] can be used jointly with the boundary identification method outlined above. The main purpose of this package is to solve, for systems without discrete nonlinearities, an equation of the form,

$$\dot{\boldsymbol{u}} = f(u(t), p), \qquad f(\cdot,\cdot), u(\cdot) \in R^n \tag{13}$$

i.e. where $f(u(t), p)$ are real functions. For most calculations it solves for steady-state solutions, $\dot{\boldsymbol{u}} = 0$, but it was decided that the algebraic solutions sequence would be used for equations defining a period-*n* limit cycle oscillation. The algebraic solution sequence solves for,

$$f(u, p) = 0, \qquad f(\cdot,\cdot), u \in R^n \tag{14}$$

which is of the form described in equation (12). From section 2.2 the equations that define a period one limit cycle can be defined as,

$$0 = \boldsymbol{c}e^{[A_2]t_1}\boldsymbol{x}(0) + \frac{\delta}{2} \tag{15}$$

$$0 = \boldsymbol{c}e^{[A_1]t_2}(\boldsymbol{x}(t_1) - [A_1]^{-1}\boldsymbol{b}) + \boldsymbol{c}[A_1]^{-1}\boldsymbol{b} + \frac{\delta}{2} \tag{16}$$

$$0 = \boldsymbol{c}e^{[A_2]t_3}\boldsymbol{x}(t_2) - \frac{\delta}{2} \tag{17}$$

$$0 = \boldsymbol{c}e^{[A_1]t_4}(\boldsymbol{x}(t_3) + [A_1]^{-1}\boldsymbol{b}) - \boldsymbol{c}[A_1]^{-1}\boldsymbol{b} - \frac{\delta}{2} \tag{18}$$

$$\boldsymbol{0} = \boldsymbol{x}(0) - \boldsymbol{x}(t_4) \tag{19}$$

For a period-*n* system the number of equations to solve becomes $4n + 8$. Additionally, extra equations have to be set up to identify the maxima of the heave, pitch and flap rotations in order to get a measure of the limit cycle amplitude i.e. an equation that isolates when the derivatives

of each degree of freedom are zero. Including this maxima identification increases the number of equations from 12 to 15, for this case.

To use the continuation method, an initial set of solutions has to be found using either a Runge-Kutta or linear methodology. From this point the continuation method can be used to vary any parameter within the system, known as the *continuation parameter,* to identify limit cycles up to the flutter boundary. A limitation at this time is that the algebraic continuation method does not allow an assessment of the stability to be made within the program unlike the continuation method for limit cycles of smooth systems of the form (13), as there is no explicit Jacobian matrix.

3 Results

The results in figures 4 and 5 show a comparison between a fourth-order Runge-Kutta scheme and the boundary identification method outlined in section 2.2. These results were generated using the Matlab functions *fsolve*, *fzero* and *fmincon*. Figure 5 clearly shows the backlash distance by the vertical separation of the linear results (marked with an asterisk). In this figure, error between the two methodologies can also be seen with the boundary identification method skipping some of the zone borders. Figure 5 also shows a point that is not in line, this is because the *fmincon* function found a maxima or minima within a linear zone, this does not, however, affect the results. In section 2.2 it states that the errors encountered are due to the methodologies requiring ranges to be set up carefully so that the next interface point is not skipped or a point at zero or negative time is not found instead. The time taken to generate both sets of results was found to be comparable but the extra time required to set up the boundary identification was far greater and, therefore, impractical.

Using the boundary identification results as a starting point, the continuation software was then used to vary parameters within the system. Figure 6 shows an initial test to assess the validity of the numerical continuation method. The results in the figure are all shown to tend to infinity as the velocity approaches the linear flutter speed ($22.8ms^{-1}$), as calculated by eigenvector analysis for the system without backlash. This result confirms the conclusions of other authors [5, 7] that state that the amount of backlash does not alter the flutter velocity. The figure also confirms that the amplitude of the LCOs varies linearly with the range of freeplay [17].

The possibility of using numerical continuation as a design tool is shown in figure 7. This figure shows the LCO amplitude and flutter velocity vary when the ratio between heave and pitch stiffness is varied. Using fraction of stiffness as a continuation parameter, the variation of LCO heave amplitude is plotted. On the damping axis, zero represents no damping and one represents the damping model used in [7]. Figure 8 shows how it is possible to use multiple parameter variation. The figure shows how the LCO amplitude varies with both velocity and damping by using multiple cross-sections as shown in figure 9. The results from these figures show how low or incorrect damping can affect the resultant motion greatly and how at certain damping levels multiple limit cycles can occur depending on the system's initial conditions. Using figure 9 at $18.4ms^{-1}$ it can be seen that above 30% damping only one limit cycle is observed whereas below this level, in general, three different LCOs are possible. Figure 10 shows that, with 50% damping, different initial conditions lead to the results converging to one limit cycle, whereas figure 11 shows different initial conditions lead to different limit cycles. In this particular case the maximum amplitudes of both oscillations are the same, as the dotted curve reaches an amplitude of 0.065 semi-chords on the negative side (see figure 12). Below the pitchfork bifurcation, at 23.5% damping, the LCOs represented by the centreline are unstable, therefore any small perturbation away from these limit cycles will result in the system converging on one of the other two possible oscillations. Figure 13 shows a detail of the folds that occur between 20% and 30% damping including stable and unstable branches.

Typical times for the numerical continuation runs are 9.5 minutes to generate 500 points on a Compaq ALPHA Server ES40 with 500MHz EV6 chips. This would typically represent 5 runs similar to that shown in figure 9.

4 Conclusion

A linear based system for identifying limit cycle oscillations in a discrete nonlinear system has been derived from a state-space model of the system. The resulting generalised solutions can be used to predict the motion of the aerofoil, including accurate capture of boundary switching points. The linear system was shown to be both robust and accurate over a range of velocities. Furthermore, the methodology proved to be computationally efficient although the inclusion of other techniques is necessary for generating starting points from which the continuation method can begin. The system has proved to be more useful than initially expected since any of

the system parameters can be changed and their effects on the resultant limit cycles examined thereby creating a useful design tool.

The limitations on the approach are that starting points must be found and, therefore, some griding of the domain must be performed in order to capture all the limit cycles. Furthermore, capturing all possible modes can become laborious as for every higher order mode, four further equations are added. It is suggested, however, that the effects of the higher order modes are less significant as damping is usually sufficient to attenuate the higher order motions in the transitionary stage. This is further confirmed in that high order modes were found not to occur in the system suggested by Conner et al. [7] which included damping from experimental work performed by the authors.

Continuation of this research will include the study of higher order modes, stability analysis of the LCOs and combining the technique with a state space representation of a transonic Euler computational aerodynamics code. This will also allow estimations of the amplitude of limit cycles throughout the flight envelope.

Acknowledgments

The authors would like to thank the Defence Evaluation and Research Agency (DERA) and the Engineering and Physical Sciences Research Council (EPSRC) for their financial support.

References

[1] T. O'NEIL, W. STRGANAC *Aeroelastic Response of a Rigid Wing Supported by Nonlinear Springs, Journal of Aircraft*, 1998, **35**(4), 616–622.

[2] I. W. KAYNES 2001 Review of aeroelasticity in the UK (Draft).

[3] M. D. CONNER, L. N. VIRGIN, E. H. DOWELL *Accurate Numerical Integration of State-Space Models for Aeroelastic Systems with Freeplay, AIAA Journal*, 1996, **34**(10), 2202–2205.

[4] A. SEDAGHAT, J. COOPER, J. R. WRIGHT, A. Y. T. LEUNG *Prediction of Nonlinear Aeroelastic Instabilities, ICAS 2000 Congress, Harrogate, UK*, 2000, 464.1–464.10.

[5] H. ALIGHANBARI, S. J. PRICE *The Post-Hopf-Bifurcation Response of an Airfoil in Incompressible Two-Dimensional Flow, Nonlinear Dynamics*, 1996, **10**, 381–400.

[6] W. B. LIN, W. H. CHENG *Nonlinear Flutter of Loaded Lifting Surfaces (I) & (II), Journal of the Chinese Society of Mechanical Engineers*, 1993, **14**(5), 446–466.

[7] M. D. CONNER, D. M. TANG, E. H. DOWELL, L. N. VIRGIN *Nonlinear Behavior of a Typical Airfoil Section with Control Surface Freeplay: A Numerical and Experimental Study, Journal of Fluids and Structures*, 1997, **11**, 89–109.

[8] J. E. JENKINS *Simplification of Nonlinear Indicial Response Models: Assessment for the Two-Dimensional Airfoil Case, Journal of Aircraft*, 1991, **28**(2), 131–138.

[9] D. TANG, M. D. CONNER, E. H. DOWELL *Reduced-Order Aerodynamic Model and Its Application to a Nonlinear Aeroelastic System, Journal of Aircraft*, 1998, **35**(2), 332–338.

[10] Y. C. FUNG *An Introduction to the Theory of Aeroelasticity, Dover Publications Inc.*, 1993.

[11] Y. S. WONG, L. LIU, B. H. K. LEE *Frequency and Amplitude Prediction of Limit Cycle Oscillations of an Airfoil Containing Concentrated Structural Nonlinearities, 42^{nd} AIAA/ASME/ASCE/AHS/ASC Structures, Structural Dynamics and Materials Conference and Exhibit*, 2001, **Paper 1293**.

[12] J. W. EDWARDS, H. ASHLEY, J. V. BREAKWELL *Unsteady Aerodynamics Medeling for Arbitrary Motions, AIAA Journal*, 1979, **17**(4), 365–374.

[13] G. H. GOLUB, C. F. VAN LOAN *Matrix Computation, John Hopkins Univerity Press*, 1983.

[14] T. F. COLEMAN, Y. LI *On the Convergence of Reflective Newton Methods For Large-Scale Nonlinear Minimization Subject to Bounds, Mathematical Programming*, 1994, **67**(2), 189–224.

[15] R. BRENT *Algorithms for Minimization without Derivatives, Prentice Hall*, 1973.

[16] E. J. DOEDEL, A. R. CHAMPNEYS, T. F. FAIRGRIEVE, Y. A. KUZNETSOV, B. SANDSTEDE, X. WANG *AUTO 97: Continuation and Bifurcation Software for Ordinary Differential Equations (with HomCont), Concordia University*, 1998.

[17] D. L. BIRDSALL *The Effects of Structural Non-Linearities on Flutter, PhD Thesis, University of Bristol, UK*, 1965.

Appendix A: Nomenclature

$[A], [A_1], [A_2]$	matrix from equation (2) in different linear regions
$[B]$	structural damping matrix
$[B_{tot}]$	combined structural and aerodynamic damping matrix
$\boldsymbol{b}$	"offset" vector associated with freeplay
$\boldsymbol{c}$	vector that isolates the nonlinear degree of freedom
$[D], [E_1], [E_2], [F_p]$	aerodynamic approximation matrices
$\boldsymbol{F}$	aerodynamic force and moment vector
$\boldsymbol{G}$	vector of eigenvalues of the A matrix
h	heave displacement
$[K]$	structural stiffness matrix
$[K_{tot}]$	combined structural and aerodynamic stiffness matrix
$[M]$	structural inertia matrix
$[M_{tot}]$	combined structural and aerodynamic inertia matrix
s_1, s_2	augmented aerodynamic states
$[V]$	eigenvectors of the A matrix
$\boldsymbol{x}$	full state vector $[\boldsymbol{y}, \dot{\boldsymbol{y}}, s_1, s_2]^T$
$\boldsymbol{y}$	state vector $[\xi, \alpha, \beta]^T$
α	pitch rotation
β	control surface rotation
δ	control surface freeplay
ξ	nondimensional heave displacement, h/b

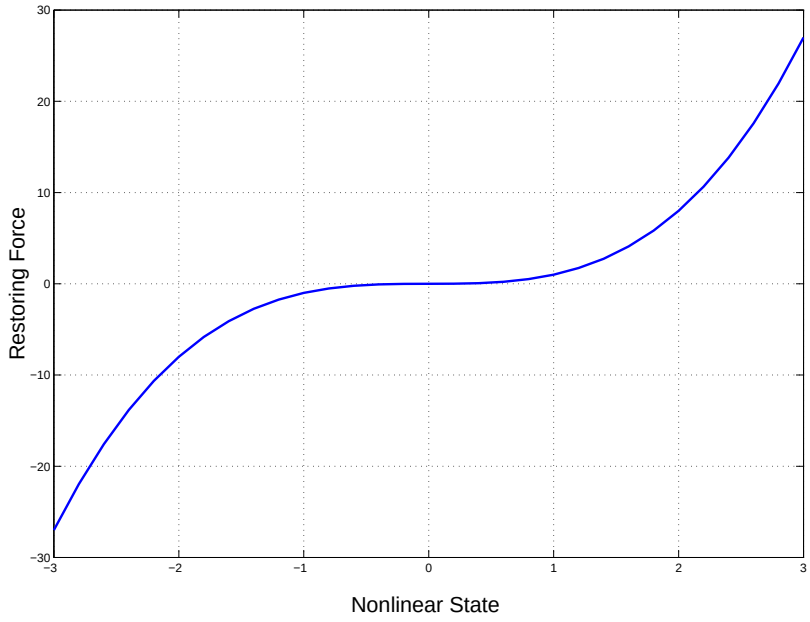

Figure 1: Cubic Nonlinearity

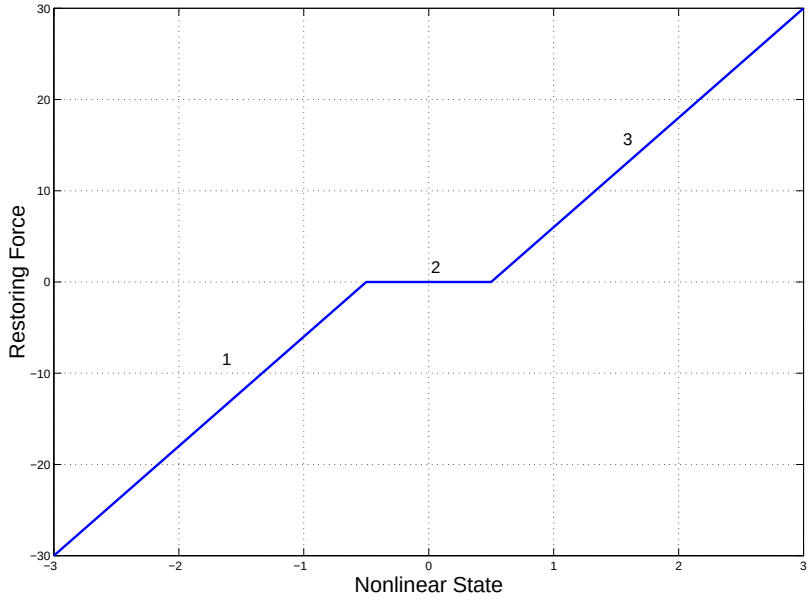

Figure 2: Freeplay Nonlinearity

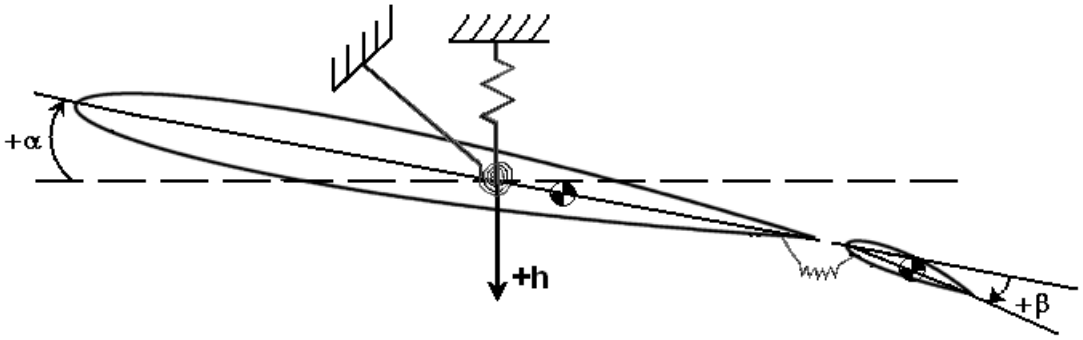

Figure 3: A 3 degree-of-freedom aeroelastic system

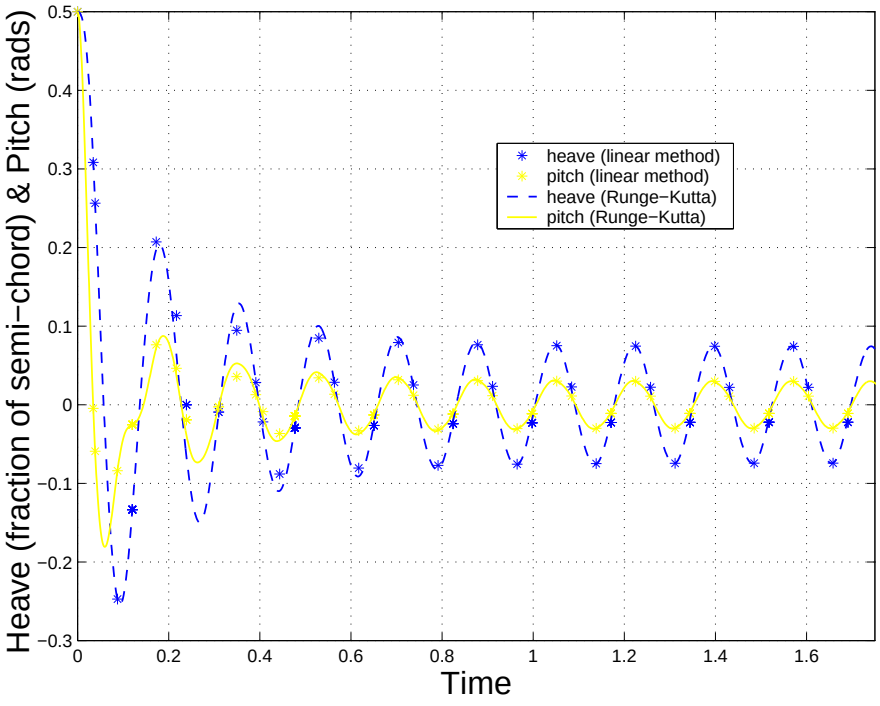

Figure 4: Pitch and Heave Motion with Time

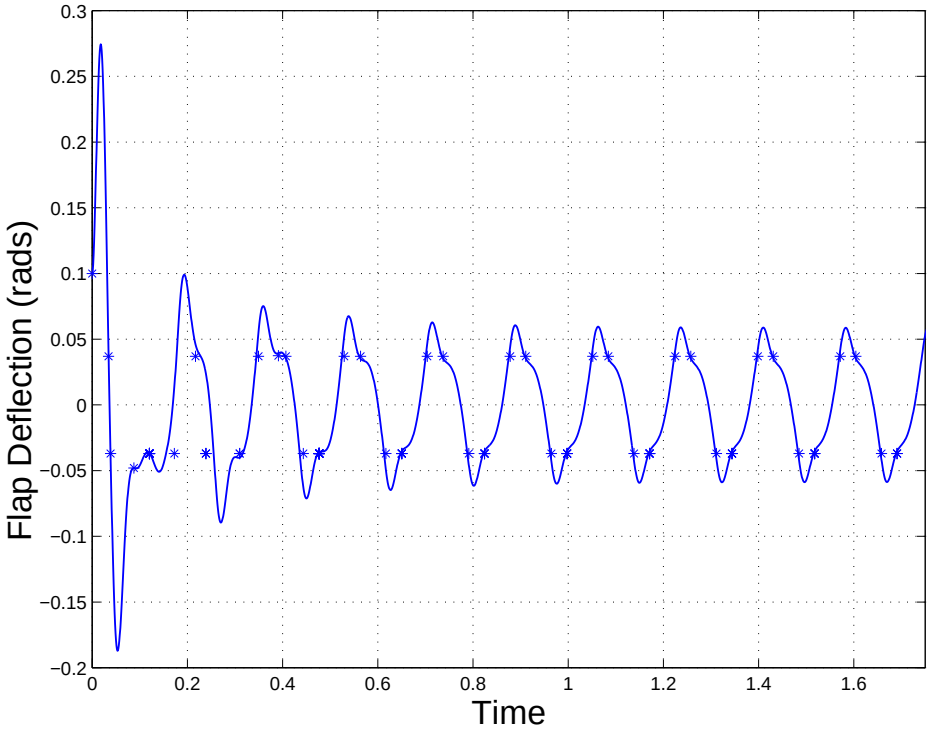

Figure 5: Flap Motion with Time

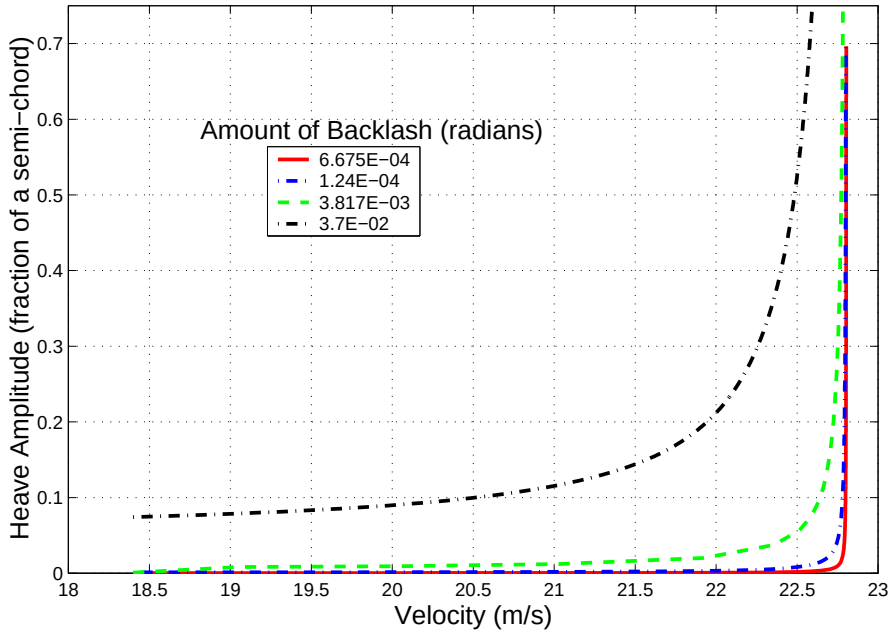

Figure 6: Effect of Backlash on limit cycle amplitude

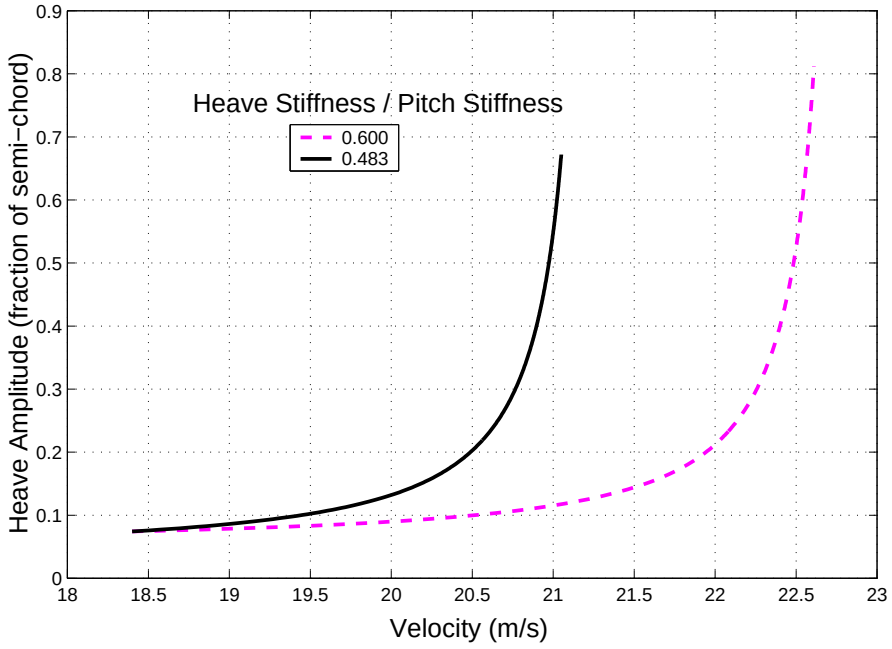

Figure 7: Effect of stiffness ratios on limit cycle amplitude

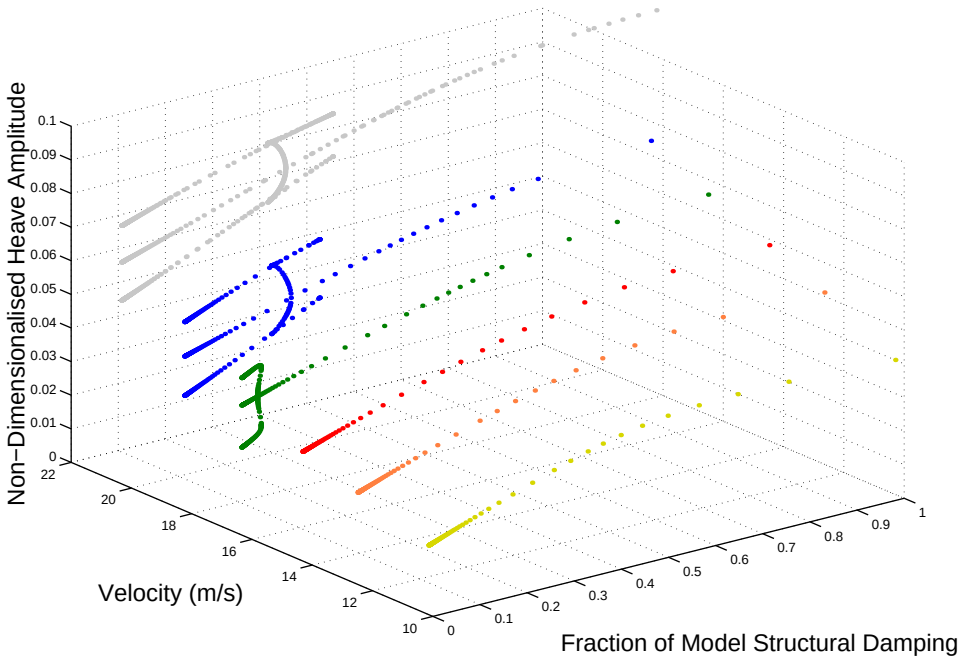

Figure 8: Variation of Heave amplitude with velocity and damping

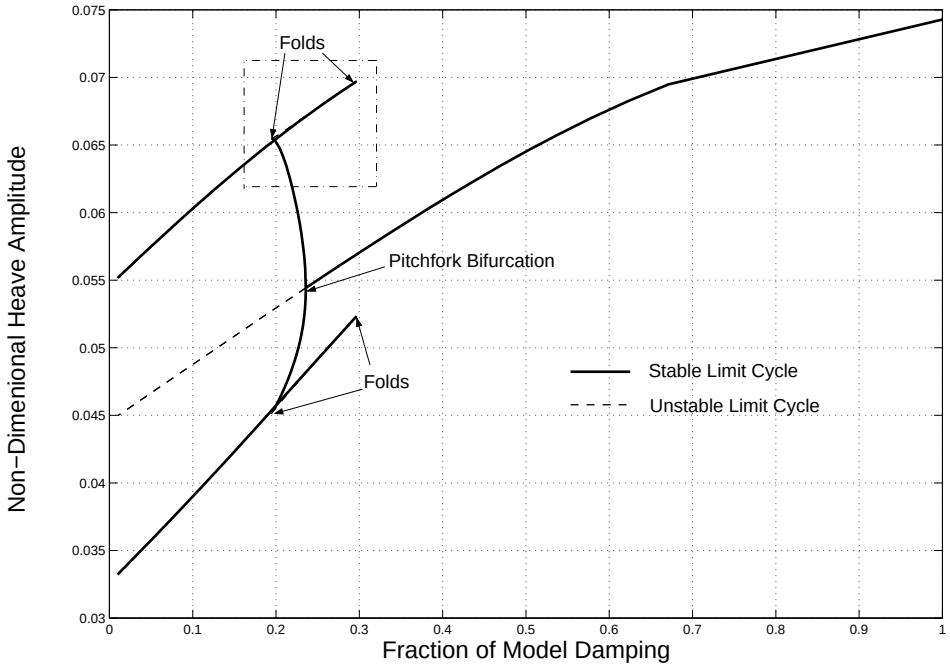

Figure 9: Variation of Heave LCO amplitude at 18.4 m/s whilst varying damping

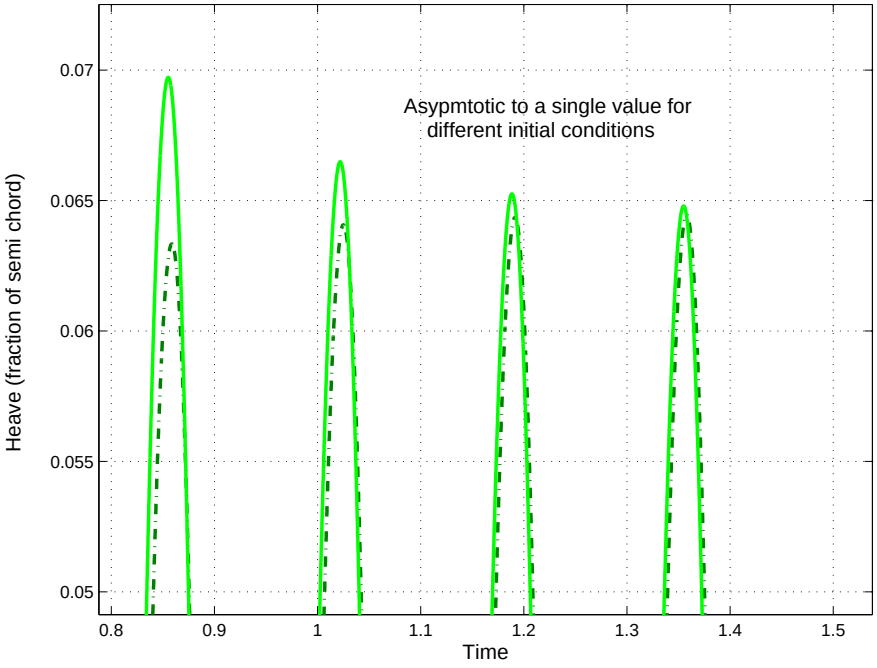

Figure 10: Runge-Kutta Results with 50% damping, detail of peak LCO amplitude

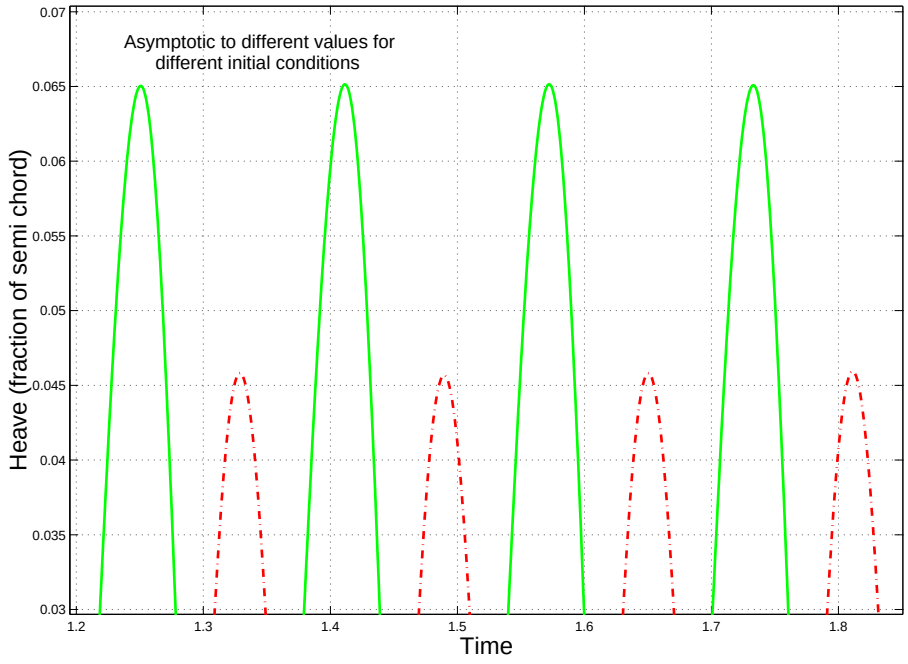

Figure 11: Runge-Kutta Results with 20% damping, detail of peak LCO amplitude

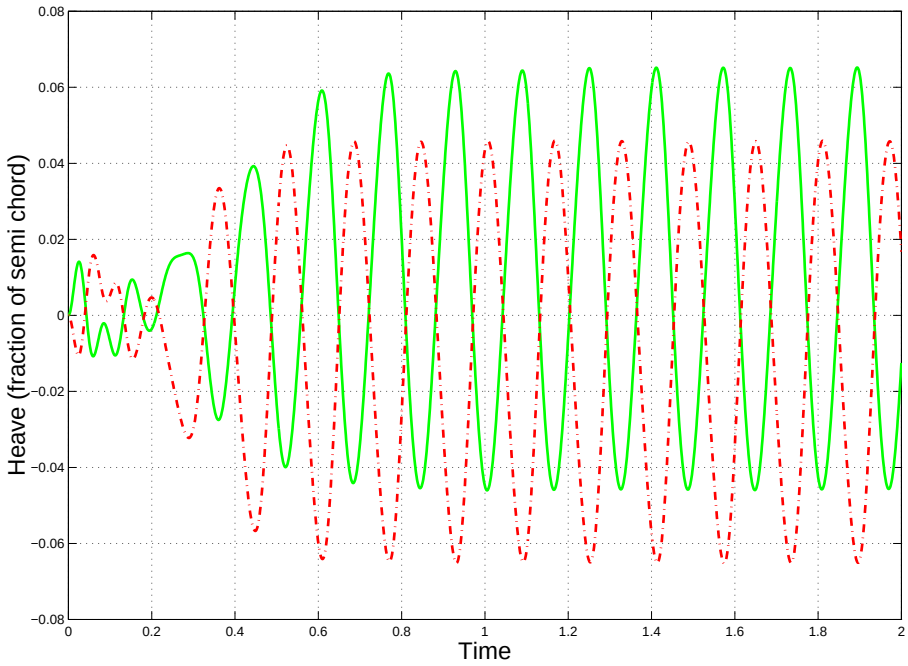

Figure 12: Full Runge-Kutta Results with 20% damping

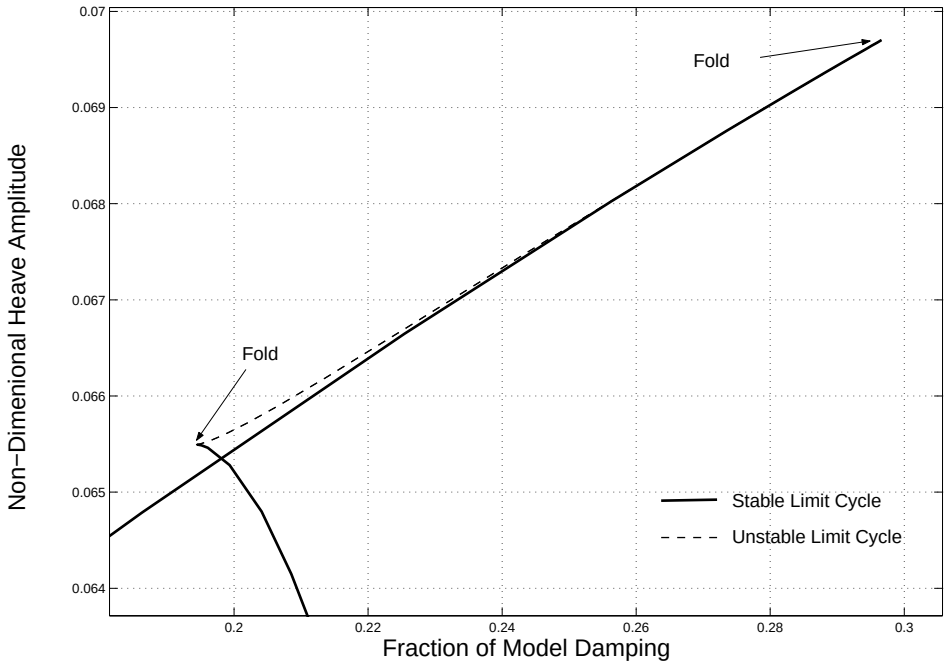

Figure 13: Magnification of figure 9 showing limit cycle stability and folds